Nonlinear Processes in Geophysics

Multifractal magnetic susceptibility distribution models of hydrothermally altered rocks in the Needle Creek Igneous Center of the Absaroka Mountains, Wyoming

M. E. Gettings

US Geological Survey, 520 N. Park Ave., Rm. 355, Tucson, Arizona 85719, USA

Abstract. Magnetic susceptibility was measured for 700 samples of drill core from thirteen drill holes in the porphyry copper-molybdenum deposit of the Stinkingwater mining district in the Absaroka Mountains, Wyoming. The magnetic susceptibility measurements, chemical analyses, and alteration class provided a database for study of magnetic susceptibility in these altered rocks. The distribution of the magnetic susceptibilities for all samples is multi-modal, with overlapping peaked distributions for samples in the propylitic and phyllic alteration class, a tail of higher susceptibilities for potassic alteration, and an approximately uniform distribution over a narrow range at the highest susceptibilities for unaltered rocks. Samples from all alteration and mineralization classes show susceptibilities across a wide range of values. Samples with secondary (supergene) alteration due to oxidation or enrichment show lower susceptibilities than primary (hypogene) alteration rock.

Observed magnetic susceptibility variations and the monolithological character of the host rock suggest that the variations are due to varying degrees of alteration of blocks of rock between fractures that conducted hydrothermal fluids. Alteration of rock from the fractures inward progressively reduces the bulk magnetic susceptibility of the rock. The model introduced in this paper consists of a simulation of the fracture pattern and a simulation of the alteration of the rock between fractures. A multifractal model generated from multiplicative cascades with unequal ratios produces distributions statistically similar to the observed distributions. The reduction in susceptibility in the altered rocks was modelled as a diffusion process operating on the fracture distribution support. The average magnetic susceptibility was then computed for each block. For the purpose of comparing the model results with observation, the simulated magnetic susceptibilities were then averaged over the same interval as the measured data. Comparisons of the model and data from drillholes show good but not perfect agreement.

Correspondence to: M. E. Gettings
(mgetting@usgs.gov)

1 Introduction

The magnetic field maps the source distribution in space as a superposition of dipolar fields on the observation surface. In geological systems, the spatial distributions of magnetic field anomalies and bulk magnetic susceptibilities are highly variable and often follow a power law distribution (Pilkington and Todoeschuck, 1993, 1995). Both can be modelled with self-affine fractals but with varying dimensions over varying scale ranges (Pilkington and Todoeschuck, 1993; Gettings et al., 1991). More recent work has shown that magnetic susceptibility distributions in the Earth can be modelled using multifractal techniques (Gettings, 1995; Lovejoy et al., 2001; Pecknold et al., 2001). Potential fields, by definition, are not fractal because they are continuously differentiable. This study is based on the hypothesis that non-differentiable magnetic susceptibility profiles reflect the spatial distribution of dipole sources in the Earth at various scales. The distribution of magnetic susceptibilities is modelled along a drillhole through altered rock, and the model is correlated with geological structures and alteration processes in the source rock.

First, the results of the measurments are discussed in the context of their relationships to metal content, alteration class, and dominant mineralogy. Next, a model of magnetic susceptibility in altered rocks is developed. The multifractal nature of the distribution of susceptibilities is demonstrated, and a simple multiplicative cascade model is seen to generate distributions very similar to the observed susceptibilities. Finally, these concepts are applied to a simple multifractal model for magnetic susceptibility in hydrothermally altered rocks, and compared with the observations. Several methods of comparing the model and data are explored to evaluate the success of the model.

2 Magnetic susceptibility measurements

For this study, 700 samples from thirteen boreholes (locations shown on Fig. 1) in the Stinkingwater district of the
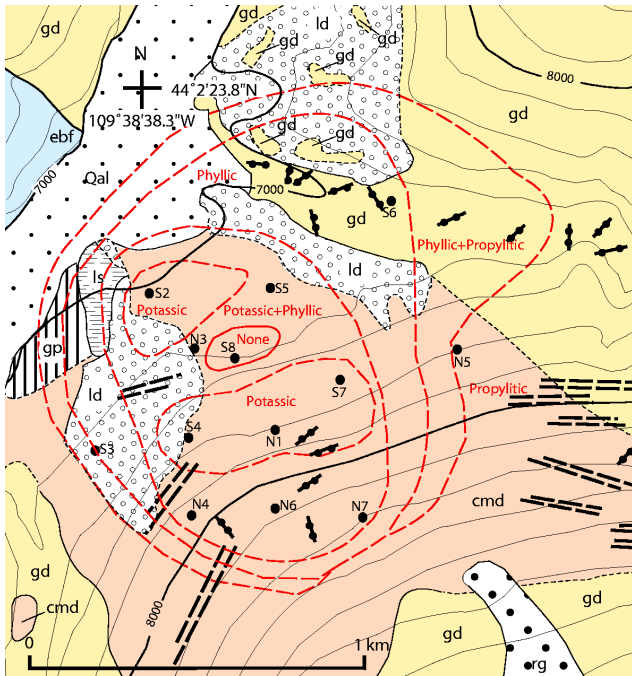
Fig. 1. Simplified geologic map of the Stinkingwater Mining region of the Needle Creek igneous center (Fisher, 1972). Rock unit abbreviations: ebf, basalt flows of the Eocene Trout Peak formation; gd, Miocene Needle Mountain granodiorite; cmd, Miocene Crater Mountain dacite; ld, Holocene landslide deposits; ls, Holocene limonitic soil; gp, Holocene gypsite; rg, Holocene rock glacier; and Qal, Holocene alluvium. Lines with two balls on them are dikes, stringers, or veins; double dashed lines are fracture systems and faults. North is to the top of the figure. The points labeled, for example, "S2" or "N1" are the locations of exploration drillholes whose core was measured for magnetic susceptibility for this study. The red overlay shows the approximate boundaries of the zones of hydrothermal rock alteration. Thin black lines show approximate topographic contour locations of altitude in ft at a 200 ft (61 m) interval.

Needle Creek igneous center in the Absaroka Range of northwestern Wyoming (Fisher, 1983) were measured for magnetic susceptibility. These samples were splits from 10 ft sections of pulverized drill core that were also subjected to chemical analyses (Fisher, 1971); thus, the susceptibility measurements represent a mean value for each 10 ft (3.05 m) interval. Studies of alteration and mineralization were also carried out (Fisher, 1983; Phelps-Dodge Corporation, 1968) so that a dataset of chemical composition, alteration class and magnetic susceptibility was obtained. This dataset may be obtained online from the US Geological Survey (Gettings, 2004).

The susceptibility measurements were made in the laboratory using a computer controlled inductive bridge instrument with a shielded coaxial sensing coil. Samples were measured in their cardboard cylindrical storage containers (about 3 cm in diameter and 5 cm in length) inserted into the measurement coil. The instrument produces a mean magnetic susceptibility and a standard deviation of magnetic susceptibil-

ity for each sample and has a measurement precision 2×10^{-7} cgs/cm^3 magnetic susceptibility (to obtain SI units of susceptibility, multiply the given cgs number by 4π). For each sample, a reading with an empty container, a reading with the sample, and a reading with an empty container were obtained, thus determining a linear drift correction with time. A single arbitrary sample was chosen as a reference and repeatedly measured throughout the duration of susceptibility measurements. This sample was measured 165 times yielding a mean magnetic susceptibility of 2.607×10^{-6} cgs/g and a standard deviation of 2.668×10^{-7} cgs/g. Susceptibility values are given per unit mass rather than per unit volume in this paper because the samples were finely ground powders.

The Stinkingwater district is a hydrothermally altered and mineralized area in the Needle Creek igneous center (Fig. 1). The rocks, alteration, and mineralization events are Eocene (approximately 40 Ma) and Upper Miocene in age (Fisher, 1983). The two intrusive units, the Needle Creek granodiorite and the Crater Mountain dacite (Fig. 1) are both altered and mineralized. The Crater Mountain dacite is most extensively mineralized in a zone where it is highly shattered (Fisher, 1972, 1983), presumably by a subsurface intrusive that was the source of the porphyry rocks. Geomorphically, the Crater Mountain dacite behaves as a fractured and incompetent unit, and displays many landslides and gravity slumps (Fisher, 1972). The dacite composition and permeability from fracturing make it a good host for hydrothermal alteration and mineralization.

The alteration pattern is a typical concentric zoned pattern (Lowell and Guilbert, 1970) ranging from propylitic in the outermost zone to phyllic alteration with patchy potassic alteration in the center (Fig. 1). The drillholes were mostly located in the more highly altered phyllic and potassic zones (Fig. 1), but several holes penetrated more than one zone vertically. Drillhole S8 penetrated 100 ft (30.5 m) in Crater Mountain dacite that is essentially unaltered. Although some alteration minerals are present (Fisher, 1972), they are volumetrically small and the rock penetrated by the drillhole is unmineralized (Phelps-Dodge Corporation, 1968). The hole thus represents a sample of unaltered rock and is inferred to represent the pre-mineralization magnetic susceptibility. Fifteen samples from this hole were measured and the results show consistent magnetic susceptibility. The measured maximum, minimum, mean, and standard deviation magnetic susceptibility were 4.78×10^{-4}, 3.18×10^{-4}, 4.03×10^{-4}, and 4.73×10^{-5} cgs/g. Thus, a value of 4.0×10^{-4} cgs/g magnetic susceptibility was taken as representative for unaltered and unmineralized Crater Mountain dacite.

The drill cores show that both alteration class and degree of mineralization vary strongly in all three dimensions in the deposit. There is also an oxidized zone and a secondary enrichment zone overlying the protore of the deposit (Fisher, 1983). Figure 2 is a log of drillhole N6 showing the magnetic susceptibility as a function of depth, together with lithologic and alteration information; the logarithm (base e) of susceptibility is used in order to observe "fine structure" at relatively low signal levels. This hole will be used here for discussion
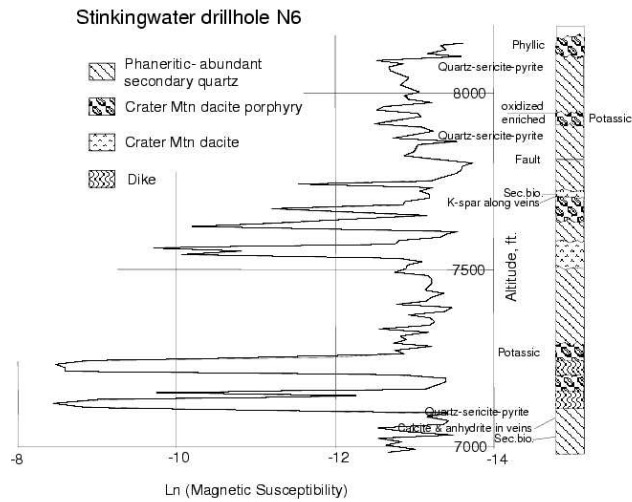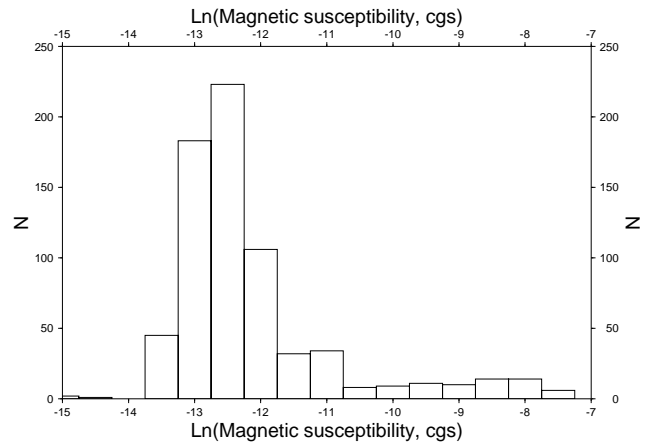
Fig. 2. Natural logarithm of magnetic susceptibility (cgs/g) for drillhole N6 (Fig. 1) plotted as a function of depth. Rock lithology, alteration, and some mineralogical information are also shown. Abbreviations are: sec. bio., secondary biotite; and K-spar, orthoclase feldspar. Note the highly variable nature of the magnetic susceptibility values.

Fig. 3. Histogram showing the distribution of the natural logarithm of magnetic susceptibility for the 700 samples from the drillholes (locations shown in Fig. 1). The distribution is multi-modal with an overlapping peaks at about –13.5 to –10.5 logarithm of susceptibility, a persistent tail from –10.5 to –7.5, and an essentially uniform distribution from –8.0 to –8.5.

because it is representative of the dataset and is the deepest hole drilled and thus the largest sample. Study of Fig. 2 shows that there is no one-to-one correlation between magnetic susceptibility and either lithology or alteration class. The two dikes have higher susceptibility but are post mineralization and not under discussion here. In general, however, areas of propylitic and phyllic alteration have relatively small values of magnetic susceptibility and areas of potassic alteration have higher values, though all are decidedly variable.

Figure 3 shows a histogram of the logarithm of magnetic susceptibility of all the measured samples. Susceptibility values are positive definite for all the minerals in this study and thus a distribution of observations with no values less than zero is expected. The distribution of susceptibilities is multimodal (Fig. 3) with a large peak at a natural logarithm of susceptibility (ln K) value of about –12.5, a smaller peak at ln K of –11, and a smaller peak at ln K values of about –7.5 to –9.0. There is a persistent tail of values between ln K equal –11 and –9. These features correspond nicely to the various rock types and alteration classes as will be shown below.

Figure 4 shows a box plot of logarithm of magnetic susceptibility plotted for the unaltered rock, each alteration class, and the post-mineralization dikes. This figure shows that the phyllically-altered rocks generally have small susceptibilities, gradually increasing through propylitic to a maximum in the potassic alteration class. Note that the susceptibility is highly variable in each class. As discussed below, it is hypothesized here that these variations are due to degree of completeness of the alteration process in each sample.

Figure 5 shows a box plot for the three classes of mineralized rocks: protore; oxidized; and enriched. As expected the protore rocks are more magnetically susceptible
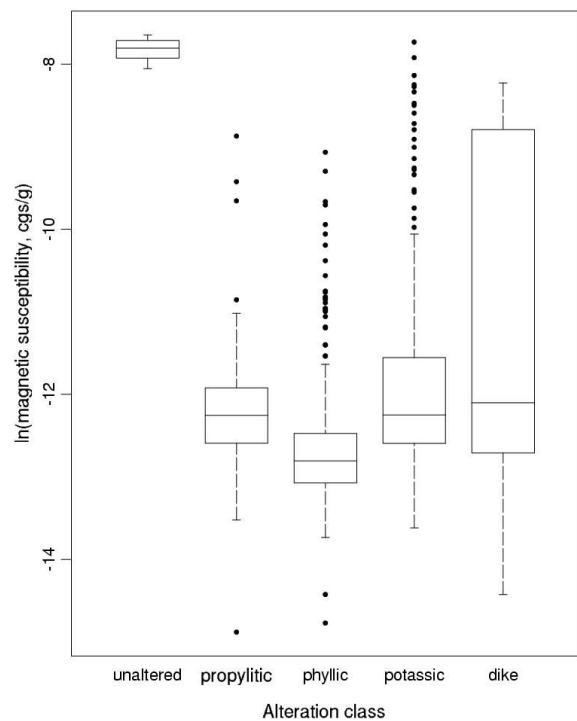

Fig. 4. Plots showing the distribution of magnetic susceptibility as a function of hydrothermal alterations. Boxplot showing the distribution of the logarithm of magnetic susceptibility for the various classes of alteration of the 700 samples. The horizontal bar in the box shows the mean, the lower and upper ends of the box show the 25% and 75% quantiles, respectively, the bars at the ends of the dashed lines show the 5% and 95% quantiles, and the solid dots show the outliers beyond the 5% and 95% quantiles.

than either the oxidized or the enriched rocks. The oxidized and enriched rocks have virtually the same magnetic
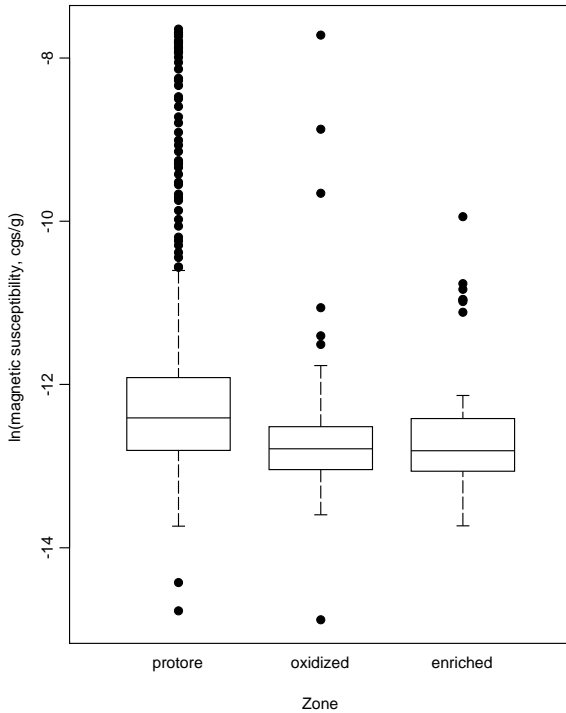
Fig. 5. Boxplot showing the distribution of the logarithm of magnetic susceptibility for the classes of secondary alteration of the 700 samples. Protore represents rocks with only primary (hypogene) alteration; oxidized represents low temperature oxidation, and enriched represents rocks from the zone of secondary (supergene) enrichment. Symbols for the boxes are as described above.
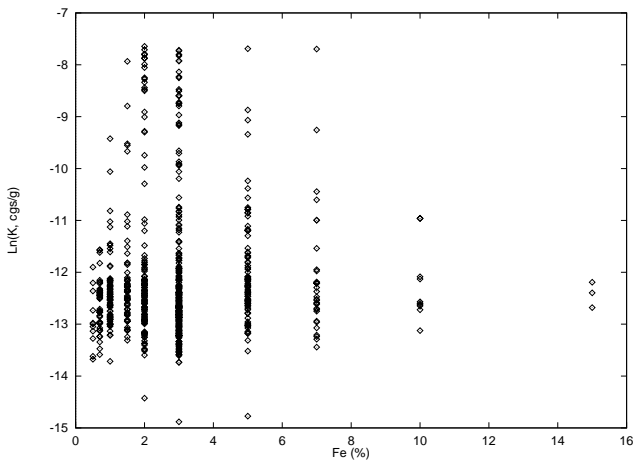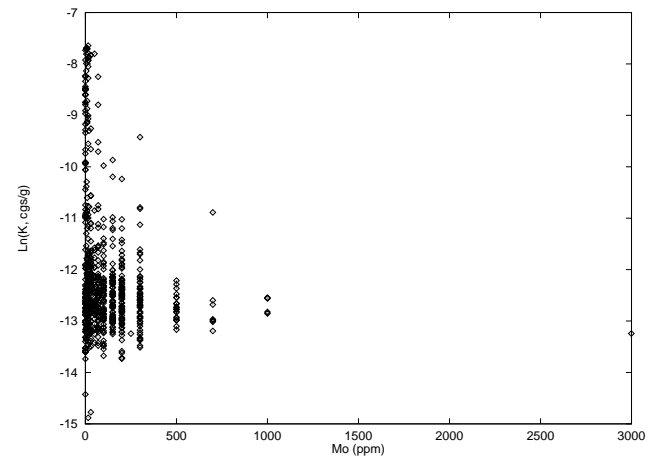

Fig. 6. Natural logarithm of magnetic susceptibility plotted as function of iron content. Iron content percent represents total iron from the sample, regardless of its oxidation state. Symbol K is magnetic susceptibility.

susceptibility characteristics because the iron bearing minerals are in low susceptibility phases in both classes. These phases are mainly hematite and pyrite, respectively.

Figure 6 shows a plot of logarithm of magnetic susceptibility as a function of total iron in the sample. This plot shows clearly that high iron content does not necessarily imply a
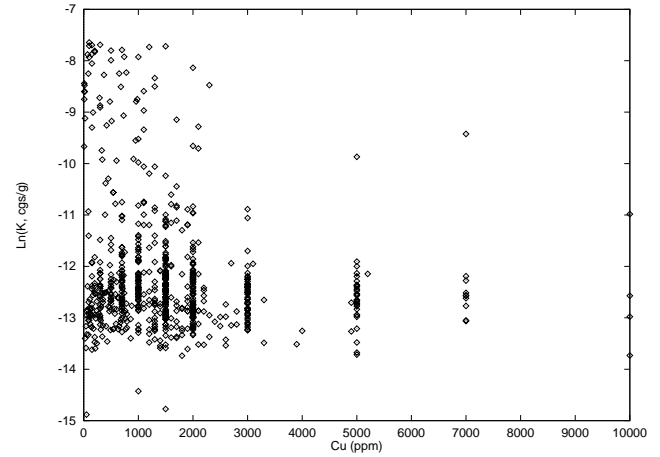
Fig. 7. Natural logarithm of magnetic susceptibility plotted as function of sample total copper content in parts per million.

Fig. 8. Natural logarithm of magnetic susceptibility plotted as function of sample total molybdenum content in parts per million.

high magnetic susceptibility; the oxidation state controls the susceptibility also. Interestingly, the degree of mineralization is not as strongly anti-correlated with magnetic susceptibility as might be expected. Figure 7 shows a plot of logarithm of magnetic susceptibility as a function of copper content, and a triangular, or perhaps peaked, distribution is observed at about 0.1% Cu. Although high copper content generally implies a low susceptibility, large variability is observed at intermediate copper contents. The minimum susceptibility values, excluding three outliers, are at chalcopyrite values (Carmichael, 1982) in the range of –13.5 to –13.8 (Fig. 7); this suggests that chalcopyrite is the principal magnetic mineral for the rocks with lowest susceptibility, as both pyrite and hematite generally have logarithms of magnetic susceptibility of –9 to –11 (Carmichael, 1982).

Figure 8 shows the distribution of the logarithm of magnetic susceptibility as a function of molybdenum content. The distribution is very similar to that for copper (Fig. 7), although the median susceptibility appears to occur more at

very small molybdenum content, as opposed to copper contents of approximately 1500 ppm. This again suggests that copper as chalcopyrite, the principal copper mineral (Fisher, 1972), is the main contributor to magnetic susceptibility in the low susceptibility rocks.

Figure 9 shows a three dimensional summary plot of the observed relationships between mineralization, alteration, and magnetic susceptibility. The general result is that the susceptibility is contained within a volume defined by the zero susceptibility plane and a peaked surface defining the observed maximum susceptibility for a given alteration class and degree of mineralization. Efforts to define the shape and controlling factors of the maximal surface have so far been unsuccessful; the discovery of the limiting surfaces is a continuing research topic. Between the limiting surfaces, the observed magnetic susceptibility distribution is discontinuous, highly variable, and fractal in nature. The samples in the phyllic class are the most dispersed in their distribution with respect to mineralization whereas those in the potassic class have the largest variability in susceptibility. The propylitic class has the most compact distribution of susceptibility with respect to mineralization.

With the relationships from Figs. 4–9, the distribution of the entire dataset in Fig. 3 is seen to be a series of overlapping sub-distributions. The large peak centered at ln K of -12.5 is mainly due to samples from the phyllic and propylitic classes, the peak at ln K of -11 is essentially due to the dike rocks, and the peak at ln K -8.5 to -8 is the due to unaltered dacite. The continuum of values of ln K -10.5 to -7.5 is principally due to the large susceptibility range of potassic alteration samples.

3 Model of rock demagnetization in a fractured porphyry system

A heuristic model of the magnetic susceptibility in the altered rocks was assumed to be the superposition of two alteration processes. First, the unaltered rocks (mainly Crater Mountain dacite) were assumed to have a constant magnetic susceptibility. These rocks were then demagnetized due to fracturing and hydrothermal alteration from the intrusion and cooling of the the porphyry, forming the volumetrically largest propylitic and phyllic zones (Fig. 1). Second, in the core of the complex and some outwardly radiating dikes, potassic alteration occurred which enhanced the magnetic susceptibility variably in the affected areas. The loss of bulk magnetic susceptibility of the altered rocks was modeled as a diffusive process from the fractures into the rock between fractures, thus allowing for variable bulk susceptibility depending on degree of fracturing and the composition and volume of hydrothermal fluids circulating through the fractures.
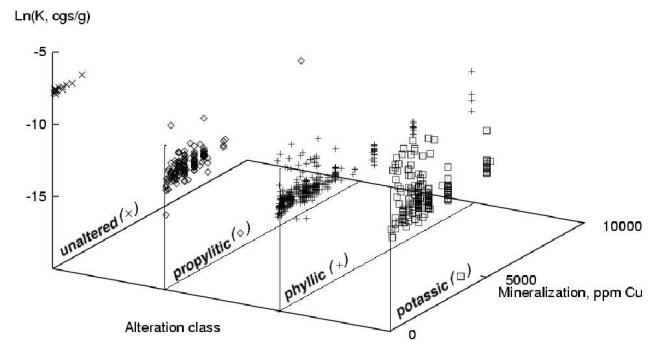

Fig. 9. Three dimensional plot of natural logarithm of magnetic susceptibility as a function of alteration class and degree of mineralization represented by total content of copper.

3.1 Basis for a fractal model

As a result of the large variability of magnetic field survey data and measured magnetic susceptibilities, several studies have applied fractal geometry techniques to magnetic field and susceptibility data models (Gettings et al., 1991; Gregotski et al., 1991; Pilkington and Todoeschuck, 1993, 1995; Pilkington et al., 1994; Maus and Dimri, 1994, 1995, 1996; Maus et al., 1997; Zhou and Thybo, 1998; Maus, 1999; Quarta et al., 2000). Most authors (e.g. Gettings et al., 1991; Pilkington and Todoeschuck, 1993, 1995; Maus and Dimri, 1994, 1995) noted that a single fractal dimension did not describe all the scales nor all datasets studied, and concluded that a self-affine fractal could only describe a limited range of scaling for a given dataset. This lack of universality led to the application of multifractals (Feder, 1988; Turcotte, 1997; Dubois, 1998; Mandelbrot, 1999) to aeromagnetic anomaly and magnetic susceptibility data. Feder (1988) hints that magnetic fields could be described by multifractal models, and Gettings (1995) showed that susceptibility data and magnetic anomaly fields from dipole sources could be well represented by simple multifractal models. Lovejoy et al. (2001) and Pecknold et al. (2001) in two seminal papers have shown that anisotropic multifractal distributions are the appropriate model for the three-dimensional distribution of magnetization in the Earth.

Multifractal measures are defined by Feder (1988) as "a distribution of physical or other quantities on a geometric support". Pecknold et al. (2001) point out that long-tailed (quasi-log normal) distributions observed for many geophysical spatial and time series constitute stable multifractal behavior and hence efforts to model such series with monofractal models is simplistic and cannot reproduce observed behavior. The spatial distribution of lithology has been modeled with fractals (e.g. Maus and Dimri, 1995; Dolan et al., 1998, unpublished modelling by the author and M. Bultman), and all authors have recognized differing fractal dimensions for differing lithologies. Multifractal models are a thus natural description for magnetic sources in the Earth's crust. Multifractal models have the property of being composed of
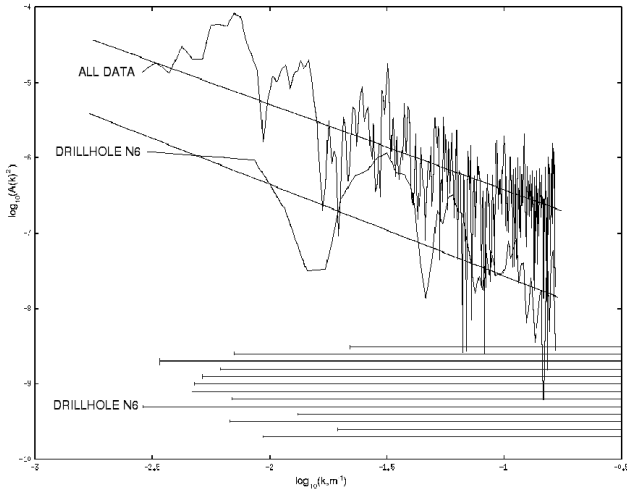
Fig. 10. The power spectrum for the ensemble averaged dataset of magnetic susceptibilities ("all data") and the deepest drillhole N6 ("Drillhole N6"). The straight lines show the global slope indicating scaling. The horizontal lines at the bottom of the figure indicate the range of data from the 13 drillholes.

fractal subsets of the support, each generally of differing dimension. In this study, the averaging of the sample over a 10 ft (3 m) interval means that all variability over scales less than 3 m is lost. Using a multifractal model accomodates this problem as simply a lack of data for scales less than the averaging interval of 3 m. The multifractal model automatically accounts for the observation that the data show different fractal dimensions depending on how they are plotted or sampled (Brown, 1995; Turcotte and Huang, 1995).

Considering the textural properties of the drillhole logs of susceptibility, one notes first that the measured magnetic susceptibility as a function of altitude (Fig. 2) is highly variable, exhibiting a positive-definite, multi-modal distribution of sharp peaks over the full range of scales of the measurements. Second, the susceptibility measurements are spatially discrete, a property precluding continuous differentiability of the observed pattern; this property is perhaps central to the operational definition of fractals and multifractals. Third, the mineral grains are distributed in a highly variable manner within rocks (Fowler, 1995), and the susceptibility is identically zero on the boundaries between grains. Because of this inherent discontinuity and since different minerals have different values of susceptibility (those with large susceptibility are termed "magnetic minerals"), the magnetic susceptibility is a function which has large variability and is not differentiable. For rock bodies, this discontinuous behavior persists from the smallest scale (mineral grains) of $\sim 10^{-5}$ m, to scales of 10^{-3} to 10^{3} m for fractures, inclusions, zones, facies, etc., up to the distribution of rock bodies (formations, intrusions, volcanic fields, etc.) at scales of 10^{0} to 10^{5} m. Thus the range of scales expected is 10^{-5} to 10^{5} m or ten orders of magnitude. These considerations indicate that a multifractal model is a good candidate for the representa-

tion of the magnetic susceptibility pattern across the physical span of the measurements. Because all minerals have some magnetic susceptibility, a support dimension of 1.0 (for a drillhole log) was assumed. This assumption ignores any voids in the rock, however the logs of the drillholes show that voids and vesicles are minimal, probably much less than 1% (Fisher, 1972).

We first apply multifractal analysis to the observed magnetic susceptibility, then to a multiplicative cascade (Feder, 1988) model, and finally to a physical model of rock alteration by chemical reaction from hydrothermal circulation through fractures. for the representation of the observations. Multifractal analysis of the observed pattern provides information on the spectrum of component fractal dimensions required to characterize the data. Following Feder (1988), the general analysis procedure is to form subsets of the dataset based on the magnitude of the susceptibility values and find the "mass" of the function in each element of each subset. The moments of the mass (the mass to an integral power, the moment order) are then summed for each subset. A sequence of mass exponents can then be defined for each moment order by finding the limit of the ratio of the logarithm of the mass moment sums to the logarithm of the subset cell widths as the cell width approaches zero. These limits yield the $f(\alpha)$ vs α curve that describes the multifractal spectrum of the data. For a multifractal, the $f(\alpha)$ curve usually assumes an inverted "U" shape with the peak value at the support dimension (1.0 for the drillhole data here). The $f(\alpha)$ values at the maximum and minimum α values define the range of the dimensions in the spectrum. The data of drillhole N6 was chosen for this analysis because it was the deepest hole (N = 114 samples, 1168 ft (358 m) total depth) and represents the best overall sample of the altered rocks in the deposit. This analysis produced an $f(\alpha)$ vs α curve with limiting dimensions of 0.4 and 1.55 and a support dimension of 1.0. Later in the study, more robust techniques for data analysis were described by several investigators (e.g. Schertzer and Lovejoy, 1987; Davis et al., 1994). These techniques were applied to determine the scaling exponents for the ensemble average of all the drillhole data (N = 700), drillhole N6, and the multiplicative cascade and diffusion-alteration model. The generalized structure function technique (Davis et al., 1994; Schmitt et al., 1995) was used for this study. The exponent function $\zeta(q)$ of the scale invariant structure function is defined by (e.g. Monin and Yaglom, 1975):

$$<|K(z+\epsilon)-K(z)|^{q}>=<|K(Z+\epsilon)-K(Z)|^{q}>(\epsilon/Z)^{\zeta(q)} \quad (1)$$

where Z is the longest scale of the scaling regime, $K(z)$ is the magnetic susceptibility as a function of depth z, q is the moment order, and the angle brackets indicate spatial averaging (expectation value). Here, the structure functions were computed from $q=0.25$ to $q=5.0$ in steps of 0.25. Plotting the logarithm of the structure function for a given q as a function of the logarithm of ϵ allows the determination of the slope $\zeta(q)$ by linear regression (Schmitt et al., 1995). The "tails" at large and small ϵ depart from a straight line because of insufficient sampling, so only the central, linear part of the

curves were used for the regression. For the ensemble averaged data, drillhole N6 and the multiplicative cascade model, a range of ϵ from 3 m to 100 m was used. Correlation coefficients for the fits for the ensemble averaged data ranged from 0.7 to 0.9; for the drillhole N6, 0.5 to 0.6, and for the cascade model 0.6 to 0.8.

### 3.1.1 Multifractal analysis of the data

Figure 10 shows the energy density spectrum for the ensemble averaged data and for the deepest drillhole N6. The straight line segments shown on the figure have a slope of $\beta = 1 + \zeta(2)$ corresponding to the global slope of the spectrum from the second order structure function. The power spectrum exhibits much more structure than the straight line, indicating differing scaling at different scales. The shape of the spectra for the ensemble and N6 are nearly identical up to characteristic lengths of about 50 m, beyond which the ensemble spectra contains two peaks not appearing in the N6 spectra. These two peaks are near the limits of the largest scales contained in the data and may not be real.

Figure 11 shows the result of estimating the scaling exponent function $\zeta(q)$ for both the ensemble-averaged data and drillhole N6. The curves show that there are significant differences in scaling between N6 and the averaged dataset although this may simply reflect better definition of the scaling from the larger (ensemble-averaged) dataset. Schertzer and Lovejoy (1987, 1991, 1997) have introduced stable and attractive universal generators for multifractal processes termed "universal multifractals". Universal multifractals model the departure from linearity of the scaling exponents with two parameters C_1 and α (Schmitt et al., 1995; Tessier et al., 1996):

$$\zeta(q) = \begin{cases} qH - (C_1/(\alpha-1))(q^\alpha - q) & \alpha \neq 1 \\ qH - C_1 q \log(q) & \alpha = 1 \end{cases} \quad (2)$$

H is the first order moment $\zeta(1)$, $0 \leq \alpha \leq 2$, α is the multifractal index, and $0 \leq C_1 \leq R$, where R is the dimension of the space and C_1 is the codimension of the mean of the process.

The parameters α and C_1 were determined by nonlinear least squares fitting of the $\zeta(q)$ function for the ensemble-averaged data. Fitting was performed using the Marquardt algorithm (Bevington, 1969) and analytic expressions for the partial derivatives with respect to the parameters. The parameter space for equation (2) for this dataset has many local minima so that numerous starting values need to be tested to find the best fit. In this case, the starting value of C_1 was taken as 0.010 and the fits were not sensitive to other starting values. Parameter α, however, was very sensitive to starting values, and initial values of 1.5, 1.6, 1.7, 1.75, 1.8, 1.9, 1.95, 1.99, and 2.0 were all tried. The resulting best fit was obtained for $\alpha = 1.735 \pm 0.003$ and $C_1 = 0.0136 \pm 0.00003$. The fit is shown in fig. 11 and is nearly identical to the ensemble-averaged scaling exponent functions. All other fits found departed significantly from the data for $q > 3.5$. The uncertainties for the fit reflect only the goodness of the fit to the data,
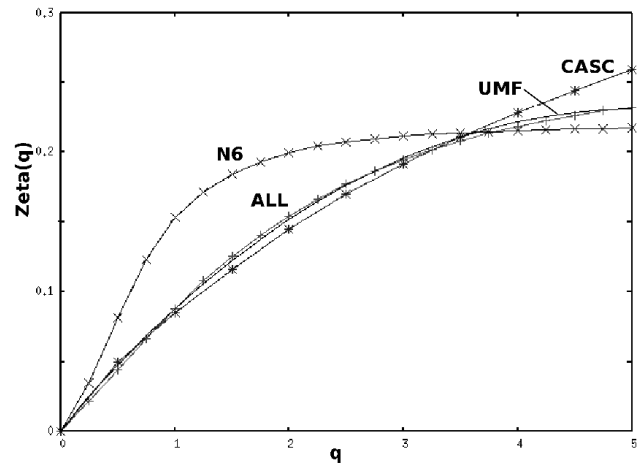

Fig. 11. Plot of scaling exponent function $\zeta(q)$ for the magnetic susceptibility data. "ALL" is scaling for the ensemble average of the entire dataset; "N6" is scaling for drillhole N6 data only; "CASC" is scaling for the multiplicative cascade model of segment lengths 0.3, 0.4, and 0.3 with proportions of 0.25, 0.55, and 0.20; and "UMF" is the best-fitting universal multifractal determined from nonlinear least squares fitting of the ensemble averaged data.

not those of the $\zeta(q)$ values for the data, which are much larger, of the order of $\pm 5\%$. At least for the data studied here, the universal multifractal is able to provide an excellent representation of the data. The α and C_1 values of 1.74 and 0.014 obtained here are significantly less than those obtained by Pecknold et al. (2001) of 1.98 and 0.047 for vertical magnetization. However, the rocks studied here are of restricted lithology and small magnetic susceptibility whereas the data investigated by Lovejoy et al. (2001) and Pecknold et al. (2001) encompass both a large variety of lithologies and magnetizations, so the the rocks studied here form a small subset of those modelled by Pecknold et al. (2001). Model fits for the data studied here that converged on α values near 2.0 all yielded poor fits to the data.

3.2 Multiplicative cascade model

Fracture distributions in rocks have been modelled with fractals (Barton, 1995; Turcotte, 1997; Dubois, 1998). For these models, the physics of fragmentation is assumed to be constant across a range of scales so that fragments fragment similar to the parent fragments; this yields the self-affine fractal behavior (Turcotte, 1997; Dubois, 1998). Fracturing can then be modeled with a segmentation model where the ends of the segments represent the fractures. Other investigators have shown that properties of the fracture system, such as aperture and length, behave as multifractals (Belfield, 1994; Bonnet et al., 2001). Moreover, multifractals appear to be a more general way to model the fracture distribution itself, because of the varying fracture response to different lithologies and heterogeneties as well as differing fracture mechanisms from different tectonic regimes (Sornette et al., 1993; Ouillon et al., 1996; Berkowitz and Hadad, 1997; Ackermann et al., 2001; Bonnet et al., 2001).
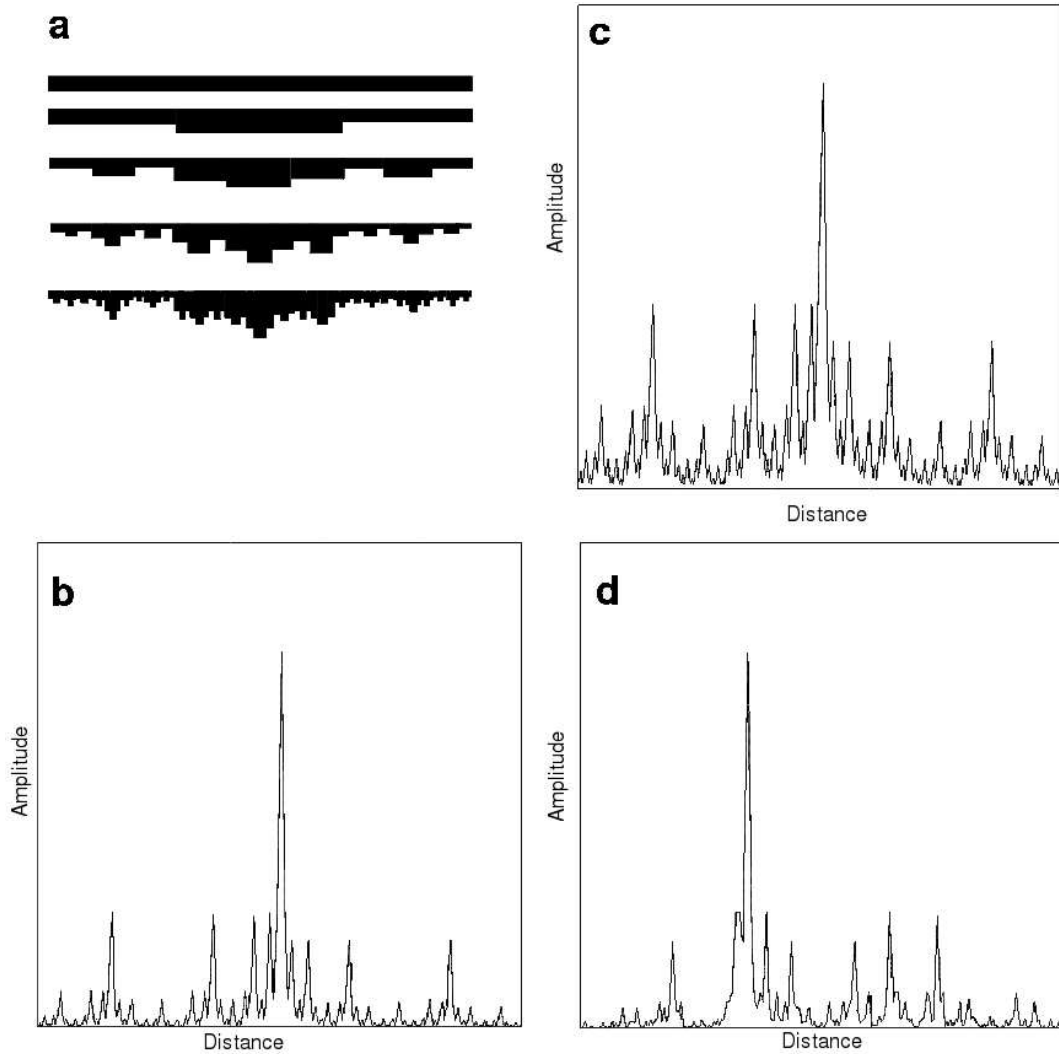
Fig. 12. Multiplicative cascade model for the depletion of magnetic susceptibility due to the alteration of the rock. (**a**) Schematic diagram of the first four generations of generalized line division for relative segment lengths of 0.3, 0.4, and 0.3 and for proportions of magnetic susceptibility into each segment of 0.25, 0.55, and 0.20. (**b**) Plot of the magnetic susceptibility after five generations with a constant order of segments at each generation. (**c**) Same plot as (b) except using a random permutation of the order of segments at each generation. (**d**) Same plot as (b) except using a random permutation of the order of the segments for the subdivision of each segment.

A simple multifractal model of the distribution of fractures and their properties can be obtained using multiplicative cascades. Numerous authors have discussed multiplicative cascades; this study followed the development of (Feder, 1988), who begins with the classic Cantor set (Cantor, 1883) and generalizes to a line division process that distributes proportions of a property (magnetic susceptibility here) into segments recursively. This process of redistribution and concentration (termed curdling by Mandelbrot (1977) and Mandelbrot (1982)) produces a multifractal. The length and magnetic susceptibility value at any stage in the process is the product of all the preceeding generations and thus is termed a multiplicative cascade. Figure 12 demonstrates the process for the case chosen here. For this model, the support dimension is 1.0, the dimension of the drillhole log, therefore the sum of the relative segment lengths must sum to unity. We

also assume that the process of redistribution of the magnetic susceptibility is conservative so that the fractions or proportions of susceptibility moved into the segments also sum to unity. A set of three segment lengths of 0.3, 0.4, and 0.3 was used, and the proportion allocated to each respective length segment was 0.25, 0.55, and 0.20. Starting with a full length line, the process subdivides it into three segments with the above-listed relative lengths and proportions. At each generation, all line segments are subdivided according to the segment lengths and proportions. For the model shown here, five generations were used.

Utilizing the proportion and length formalism just described, the exponent of the proportions q (Feder, 1988) is a free parameter called the moment order, and in order for the measure to remain finite, this results in constraints on the exponent of the lengths which is related to the fractal

dimension (Feder, 1988). Generalizing to any number of segments yields the defining equation

$$\sum_{i=1}^{N} p_i^q l_i^{\tau(q)} = 1 \tag{3}$$

For given values of q, $\{l_i\}$, and $\{p_i\}$, Eq. (3) is solved numerically to yield the sequence of mass exponents $\tau(q)$ (Feder, 1988). Once the sequence of mass exponents has been obtained, the $f(\alpha)$ vs α curve can be obtained as described previously. As shown in Feder (1988), the line division and proportioning process produces a multifractal which has a spectrum of dimensions. The support dimension, that is, the dimension of the segments on which the property is proportioned, can be either fractal or Euclidean (Euclidean is a particular fractal dimension that is integer and includes the whole space associated with that dimension). Moreover, the set of proportioned property is also fractal as are its subsets; for the data described here the 3 m averaged samples are one such subset.

On the plots (Fig. 12), the ordinate is the proportion in the line segment plotted at the center of the segment. Although in b) of the figure, the pattern is quite variable similar to the magnetic susceptibility data (Fig. 2), it still has too much symmetry when compared to the observed data. This can be further randomized by randomly choosing the order of segments (and accompanying proportions) at each generation (Barton, 1995; Dubois, 1998). Part c) of Fig. 12 shows the result of one such simulation. This pattern is closer to that observed but still too symmetric. Finally, part d) of Fig. 12 shows the results of going one step further, randomly choosing the order for each segment as it is subdivided and proportioned. This process produces distributions that look the most like the observed distribution of magnetic susceptibilities measured in the drillholes.

The scaling exponent function $\zeta(q)$ was determined from the multiplicative cascade model using generalized structure functions as describe above. The results, shown on Fig. 11, fit the ensemble-averaged data surprisingly well up to q values of about 3.7. This is especially true as no fitting algorithm was used other than running a few dozen simulations and choosing the one visually most similar to a plot of the magnetic susceptibility for drillhole N6.

For this discussion, we have considered only a one-dimensional (Euclidean) system, such as measurements of physical properties in a drillhole or along a profile. The segmentation scheme can be easily generalized to two or three dimensions if one assumes the distribution in each dimension is independent of the others; then, the desired distribution is just the product of three distributions, one for each spatial coordinate. This may be appropriate for applications such as particle concentration (metal concentration in a deposit, sediment detritus, etc.; see also Turcotte (1997) and Dubois (1998) but unsuited for features such as fractures or sedimentary beds which are correlated between dimensions. In these cases, one must know the form of the correlation in order to carry the one-dimensional case into two- or three-

dimensions. Finally, note that several different line division processes can be superposed either concurrently or serially to model, for example, syngenetic or successive tectonic events.

Proportions that add to unity have been used in the examples here. This case conserves the total amount of the property distributed on the segments, and in such a case the proportions on the segments have a one-to-one correspondence with the probability of being in any segment. However, this normalization criterion is not essential and a sum of proportions less than unity can be used to model a system which is losing a material property and proportions greater than one can model a system acquiring a material property. When modeling open systems in this way care must be exercised in the calculation of the spectrum of dimensions. Although the sequence of mass exponents q vs $\tau(q)$, (Feder, 1988) can be calculated in the same way, the formula for the spectrum of dimensions assumes the sum of proportions is unity and must be modified for the open system case.

3.3 Rock alteration model

The multiplicative cascade model described above is somewhat superficial in that it does not explicitly model the alteration of the rocks leading to a reduction in magnetic susceptibility. Accordingly, a model that explicitly models the rock alteration and attendant susceptibility reduction was attempted. A fractal or multifractal distribution of fractures was assumed, and the (multifractal) distribution of magnetic susceptibility was calculated as the spatial average susceptibility of each block of rock between two fractures. Alteration of the wallrock inward from each fracture is assumed to occur by processes controlled by the diffusion equation:

$$\partial C / \partial t = \kappa \nabla^2 C , \tag{4}$$

where C is the degree of alteration and κ is the diffusion coefficient. The loss of susceptibility is modeled by using the diffusion equation solution for a half space. The degree of magnetic susceptibilty loss K/K_0 is assumed to be proportional to the degree of alteration. For a constant initial magnetic susceptibility K_0, and an efficiency factor E, one obtains

$$K/K_0 = 1 - E[1 - erf(x/2\sqrt{\kappa t})] \tag{5}$$

The efficiency factor E can take values between -1 and 1 for various kinds of models, negative values for aggregation and positive values for depletion. For this study, E was taken as 1. Equation (5) thus defines the magnetic susceptibility for a block for alteration from a single fracture inwards from the fracture; it is used on each side of each rock block in the model. The bulk magnetic susceptibility of each block (segment) is then the integral mean of the susceptibility as a function of distance from the bounding fractures. For larger blocks, the mean susceptibility will be larger if the fluid circulation did not go on for a long enough time for the entire block to be completely altered.

If the process runs only for a short time, only a small amount of rock would be altered immediately adjacent to
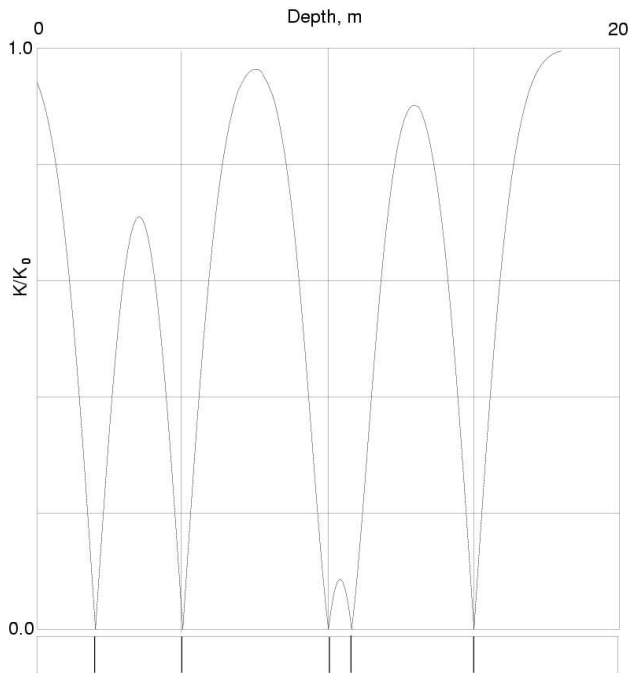
Fig. 13. Model for hydrothermal alteration of wallrock by diffusion from hydrothermal fluids circulating through fractures. Vertical lines in the bar at the bottom of the figure show the location of the fractures. Plot shows the decrease in magnetic susceptibility approaching a fracture as the ratio of the diffusion-controlled susceptibility to an assumed pre-alteration susceptibility (K/K_O). For each block between two fractures, the mean magnetic susceptibility is the integral mean of K/K_O for the block.

each fracture; and if the process runs for a long time, essentially all the rock would be altered to a low magnetic susceptibility value. For intermediate times, a complex pattern of susceptibility will occur governed by the sizes of the blocks (fracture distribution) and the rate of reaction. Large blocks of rock that have greater distance between fractures take longer to alter completely, and thus are the last to lose their magnetic minerals. Figure 13 shows a simulation for a few fractures. The bar at the bottom of the figure shows the location of the fractures, and the curves above show the remaining magnetic susceptibility through the blocks. The maximum susceptibility in a block is controlled by the fracture spacing, and close spacing leads to small susceptibility. The rightmost block has a large spacing to the next fracture (off the diagram) and the susceptibility in the center of the block is seen to be unaltered from the starting value.

3.4   Model simulations and comparison to N6 data

For the model shown here, two fracture distributions were used: the distribution of actual fractures from profiles across a homogeneous rock was used to obtain a fracture distribution ("pavement 1000", Barton, 1995, p.161); and the distribution of fractures from the segment ends of the multiplicative cascade model described above. The distribution of fractures from both are very similar and when the model results
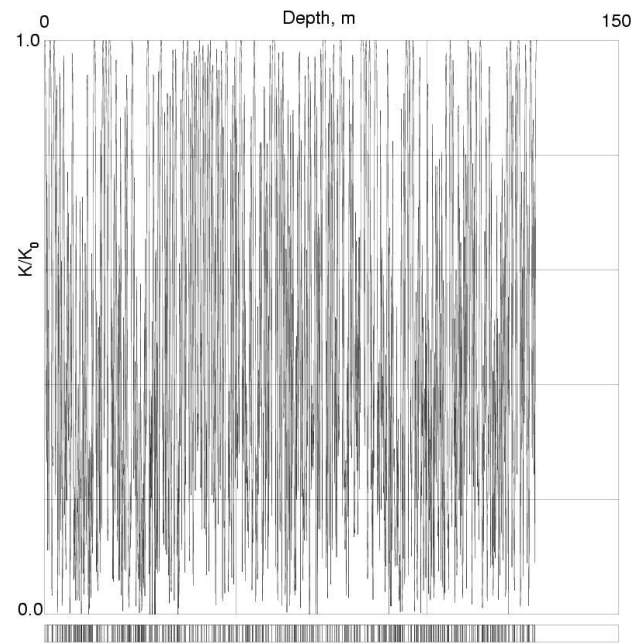

Fig. 14. Model of magnetic susceptibility as in Fig. 13 for a distribution of fractures at a scale appropriate for the data of drillhole N6 (Fig. 2). As in Fig. 13, the bar at the bottom of the plot shows the locations of the fractures.

are averaged to the 3 m interval of the data, the results are identical.

The magnetic susceptibility in each segment is assumed to have started at a constant homogeneous value for the host rock (the Crater Mountain dacite, Fisher, 1972) and then been systematically reduced due to the alteration process from reactive fluids circulating through the fractures and altering the wall rock of the fractures. The process is assumed to be oxidizing so that the magnetic susceptibility is lowered in proportion to the degree of alteration. Thus, the model applies to the propylitic and phyllic alteration stages but not the potassic stage that enhances magnetic susceptibility.

Figure 14 shows a simulation applied to the whole fracture set and the resulting highly variable magnetic susceptibility distribution. The plotted magnetic susceptibility ratio for each segment (Fig. 14) is the integral mean of the susceptibility in each block. The alteration rate (diffusion coefficient) and time of fluid flow have been arbitrarily chosen to leave the thickest intervals of rock essentially unaltered at their centers. When averaged over 3m intervals analogous to the observations (Fig. 15), the simulation is very similar to the distribution of susceptibilities observed in the parts of the drillhole not affected by potassic alteration or subsequent dike emplacement (compare the distribution of the model susceptibilities Fig. 16 to the observed data, Fig. 3). The potassic alteration enhances susceptibility in this system because it is a reducing environment resulting in magnetite series iron minerals instead of hematite. The two dikes are mafic in composition and so have a relatively high susceptibility. Further applications of this model using
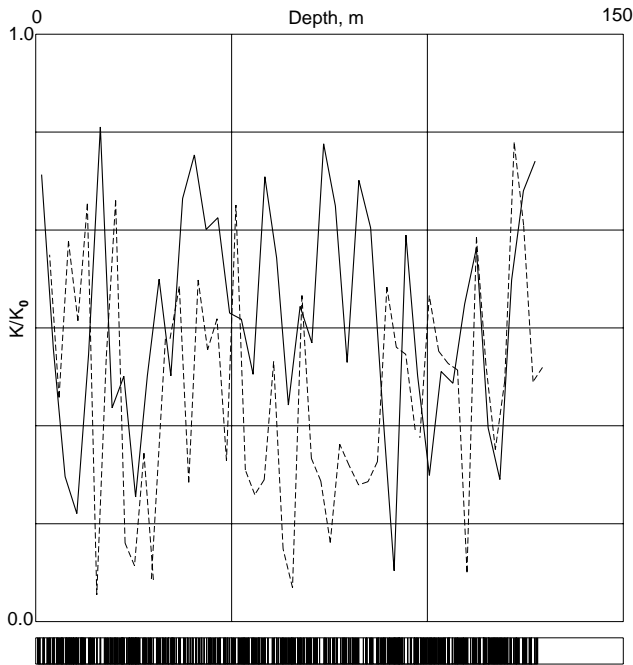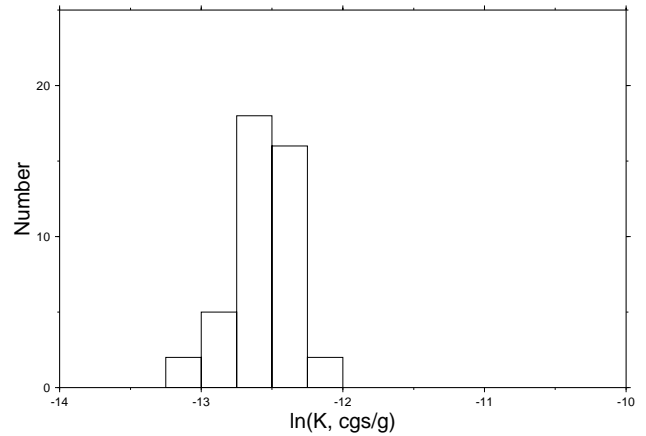
Fig. 15. Model of Fig. 14 averaged over 3 m interval to match the samples of this study and scaled to match observed susceptibility values. Solid line is the averaged model of Fig. 14, and the dashed line is the data of drillhole N6 from the phyllic and propylitic zones shown for comparison. The data have been arbitrarily shifted vertically for figure readability. Note the statistical similarity in susceptibility peak amplitudes, shapes and variability between the model and data.

Fig. 16. Histogram showing the distribution of the natural logarithm of magnetic susceptibility for the averaged model values. Compare to distributions for the observed data in Figs. 3 and 4.

Fig. 17. Plot of the scaling exponent function $\zeta(q)$ for rocks from the phyllic and propyllitic alteration classes from drillhole N6 and for the alteration model.
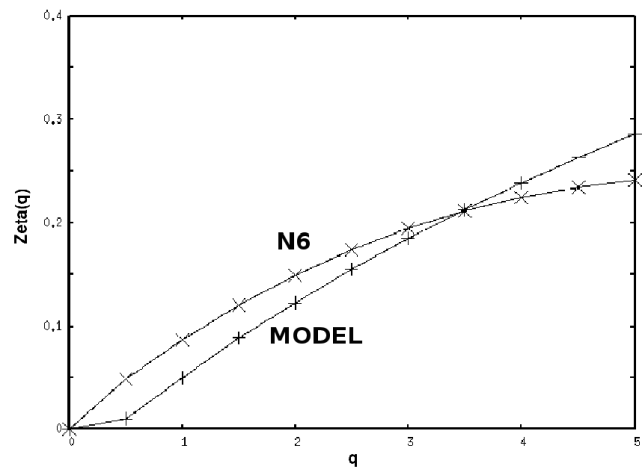
experimentally determined diffusion coefficients appropriate for the dacite might allow some constraints to be placed on the effective time of circulation of altering fluids and estimate reaction rates.

Figure 17 shows the scaling exponent function $\zeta(q)$ for the phyllic and propylitic alteration class rocks of drillhole N6 and for the diffusion-equation controlled model averaged to the 3 m interval of the data. The fit between the model and data is not bad considering that no adjustment of the degree of alteration of the blocks has been attempted in order to achieve a better fit. Such an exercise might be unwarranted because there is no information in the data on fracture aperture nor the amount of hydrothermal fluid circulation, and the 3 m averaging interval smooths the data in any case.

Several investigations were made to quantify the similarity of the model and data (Fig. 15). The model cannot be fit exactly to the data because the actual locations of fractures is unknown and cannot be deduced from the averaged data. To be judged good, the model must produce nearly the same variability, number of peaks and troughs with closely similar widths. The distribution or clustering of amplitudes as a function of depth must also be comparable and this variation is not accounted for in statistical models. Three mathematical test functions with identical mean and standard deviation for the whole 700 point dataset were used to gain insight into

discriminating between functional behaviors, that is, to determine how "similar" two datasets might be. The functions used were a straight line, a sine function, and a fractional Brownian motion fractal, shown in the first frame of Fig. 18. For this study, two integral measures and three moving window measures were used to characterize datasets. The integral measures were the variation (Tricot, 1995) of a function $z(t)$:

$$V(\tau) = \int_a^b rng(z(t))dt, \tag{6}$$

where $rng(z(t))=sup\{z(t')-z(t'')\}$ and t' and t'' belong to $[t-\tau, t+\tau]$; and the (second order) structure function (Tricot, 1995):

$$S_n(\tau) = \int_a^b |z(t+\tau) - z(t-\tau)|^n dt, n = 2 \tag{7}$$
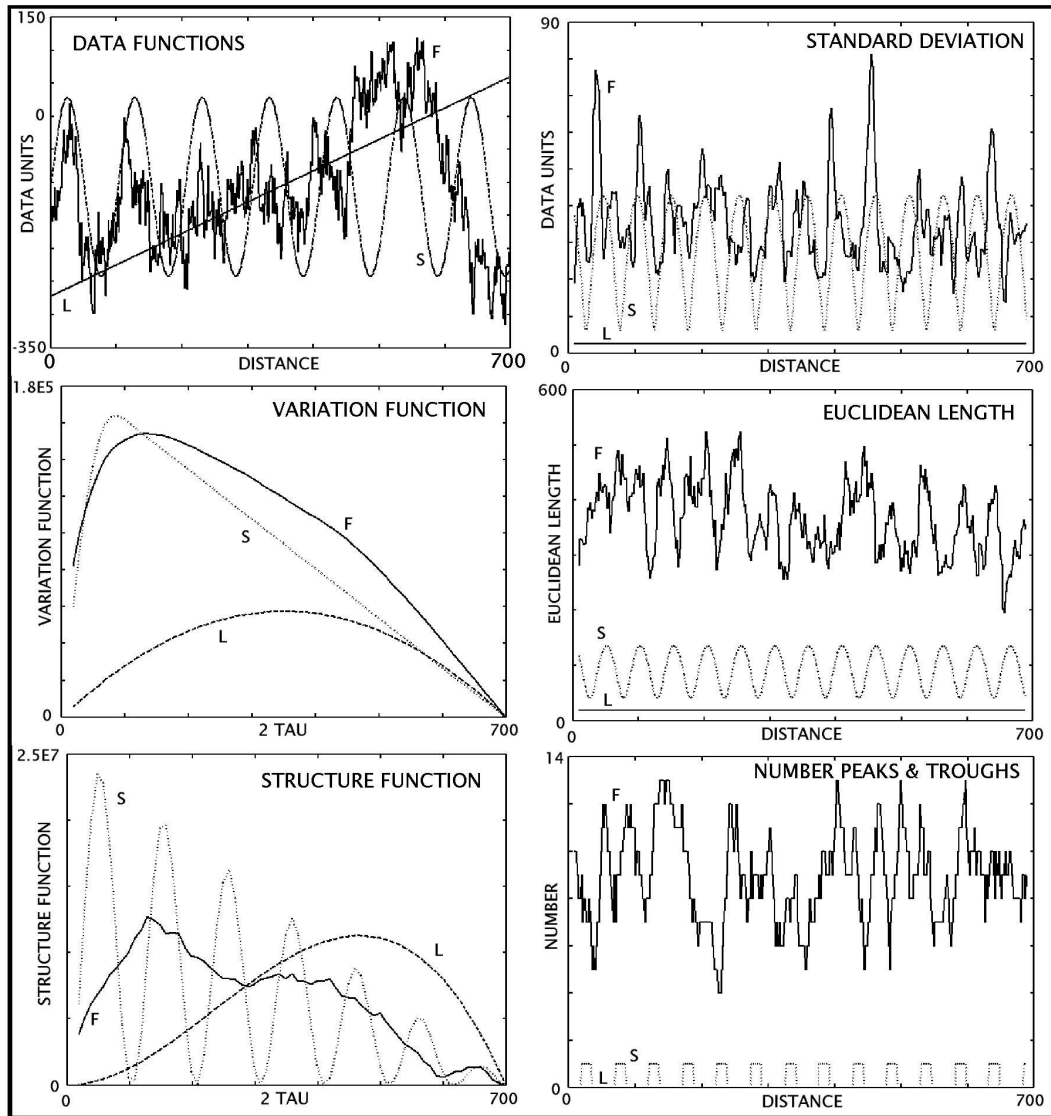
Fig. 18. Plots of three test functions (straight line, L; sine function, S; and fractional Brownian motion fractal, F) and five measures used to compare them. The variation and structure functions (see text) are integral functions of the window width (2τ) whereas the standard deviation, Euclidean length, and number of peaks and troughs are moving window functions for a 10 point wide window.

These two measures discriminate strongly between functional forms and are shown for the test functions in Fig. 18. The variation shows the behavior of the dataset at varying window widths, as does the structure function. However, the structure function has the additional property of being zero at tau (half window width) values equal to periodicities in the dataset investigated (see the structure function for the sine function case, Fig. 18). Thus, minima in the structure function suggest important "wavelengths" in the dataset. Both functions appear to discriminate well between the test functions. To characterize dependence on the abscissa, three moving window functions were used to compare datasets: the standard deviation, number of peaks and troughs, and the Euclidean length (the total length of line segments connecting the datapoints in the window). Gettings (2002) discusses the robustness of the number of peaks and troughs and Eu-

clidean length as textural measures and shows that selecting the smallest window width of interest preserves all information present in larger windows. In this study, a window width of 10 points was used. Figure 18 shows the results of these three window functions for the trial functions. Clearly, all three contain important information about the data, and at least for the fractal case, the measures are essentially independent of each other.

Figure 19 shows the results of computing the five measures for the model and data curves of Fig. 15. Although in general the two curves are quite similar for each of the five measures, there are some systematic differences the shape of the variation (data flattens off at smaller tau more quickly than the model) and the structure function shows that the model has a slightly larger range at all tau than the data. The behavior of the standard deviation is quite similar for both the model
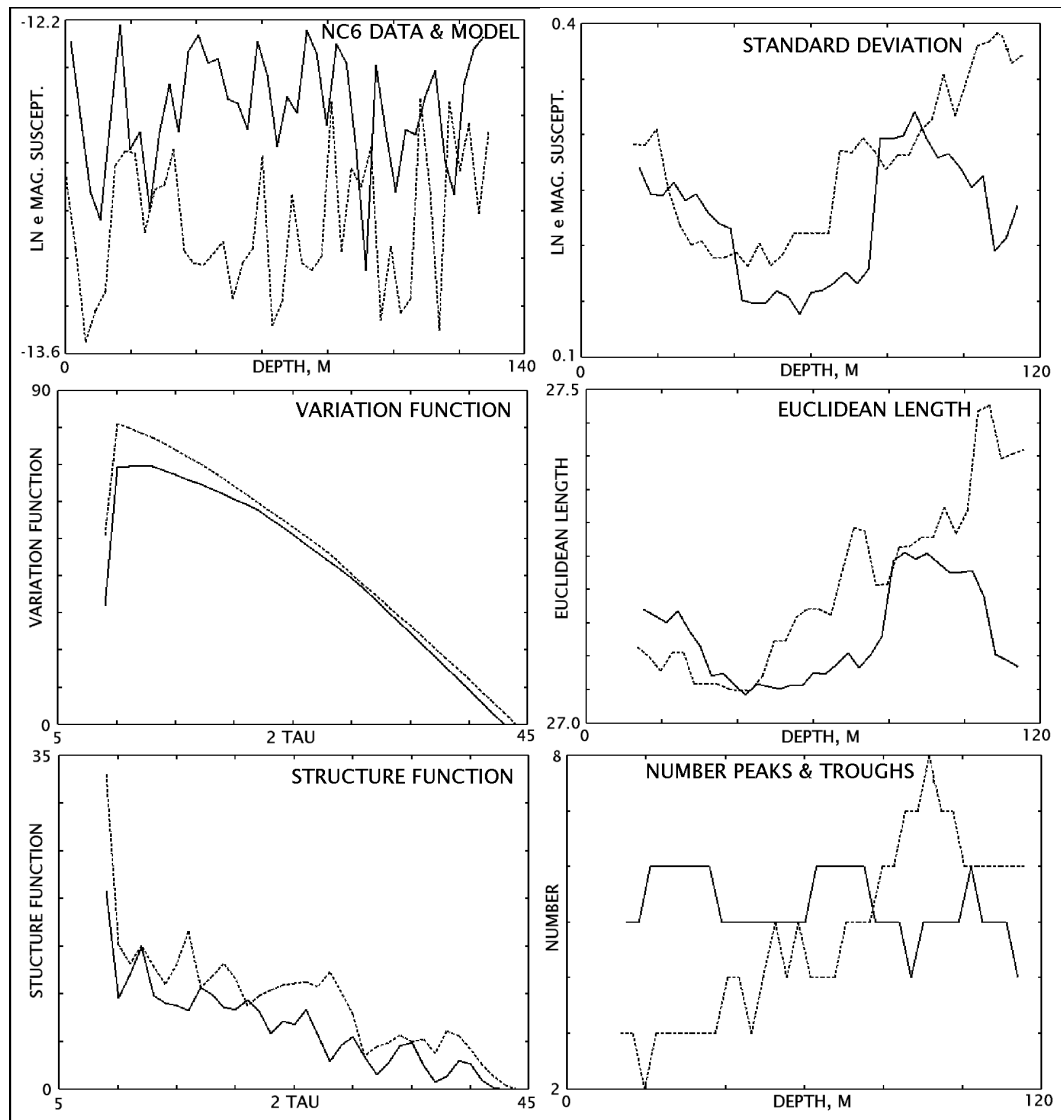
Fig. 19. Plots of the data (solid lines) and model (dashed lines) and the five comparative measures used to evaluate the similarity of the data and the model for depletion of magnetic susceptibility due to hydrothermal alteration in a porphyry system.

and data, however Euclidean length is generally larger for the model compared to the data, as shown also by the structure function. The number of peaks and troughs plot reveals that although the model and data are the same on average, the model systematically increases with depth whereas the data do not. The measures of Fig. 19 appear to be a sensitive and discriminating method of comparison of "noisy" data.

4 Conclusions

The Stinkingwater porphyry copper-molybdenum deposit has a complex, multi-fractally distributed magnetic susceptibility. The distribution of the logarithm of magnetic susceptibility is multi-modally distributed. The peaked distributions of logarithms suggests a multiplicative process for depletion of susceptibility. The logarithm of magnetic sus-

ceptibility of rocks subjected to phyllic and propylitic alteration is distributed in overlapping peaks; those with potassic alteration form a tail toward higher susceptibility, and the unaltered source rocks in this study are approximately uniformly distributed across a narrow range in logarithm of magnetic susceptibility. There is no systematic relationship between degree of metalization and magnetic susceptibility. In general, the more highly mineralized rocks have lower susceptibility, however the susceptibility is highly variable at all grades. The averaging of the drill core samples over 10 ft (3 m) intervals precludes any more precise description of the distribution of magnetic susceptibility.

The distribution of magnetic susceptibility for the ensemble-averaged data and in the deepest drillhole (the largest number of samples) has been shown to exhibit multifractal behavior, with a scaling exponent function

that is closely modeled with the universal multifractals of (Schertzer and Lovejoy, 1987).

The multifractal distribution is hypothesized to be due to a multifractal distribution of fractures that were the source of the alteration caused by hydrothermal fluids circulating through the fractures. Incomplete alteration of wall rock farther from the nearest fracture explains the high variability of susceptibility. The resulting model has scaling and statistical properties that are similar to the observed data, including the model distribution of logarithm of magnetic susceptibility (Figs. 3 and 16). Several measures, including the variation and structure functions and moving window functions of standard deviation, number of peaks and troughs, and Euclidean length have been shown to be sensitive discriminators of statistical similarity for these data.

Multifractal models of fractal random logarithmic or $1/f$ noise as described by Mandelbrot (1999) may be appropriate for describing this data. Although not normally distributed under the logarithmic transformation, the data are certainly peaked and appear to satisfy the central limit theorem (Jeffreys, 1961). This implies that they can be modeled by multiplicative processes as described in this paper.

References

Ackermann, R., Schlische, R., and Withjack, M.: The geometric and statistical evolution of normal fault systems: an experimental study of the effects of mechanical layer thickness on scaling laws, J. Struct. Geol., 23, 1803–1819, 2001.

Barton, C.: Fractal analysis of scaling and spatial clustering of fractures, in: Fractals in the Earth Sciences, edited by: Barton, C. and LaPointe, P., Plenum Press, New York, 141–177, 1995.

Belfield, W.: Multifractal characteristics of natural fracture apertures, Geophys. Res. Lett, 21, 2641–2644, 1994.

Berkowitz, B. and Hadad, A.: Fractal and multifractal measures of natural and synthetic fracture networks, J. Geophys. Res., 102, 12 205–12 218, 1997.

Bevington, P.: Data Reduction and Error Analysis for the Physical Sciences, McGraw-Hill, New York, 1969.

Bonnet, E., Bour, O., Odling, N., Davy, P., Main, I., Cowie, P., and Berkowitz, B.: Scaling of fracture systems in geological media, Rev. Geophys., 39, 347–383, 2001.

Brown, S.: Measuring the dimension of self affine fractals: the example of rough surfaces, in: Fractals in the Earth Sciences, edited by: Barton, C. and LaPointe, P., Plenum Press, New York, 77–87, 1995.

Cantor, G.: Grundlagen einer allgemeinen mannichfaltigkeitslehre, Mathematische Annalen, 21, 545–591, 1883.

Carmichael, R.: Magnetic properties of minerals and rocks, in: Handbook of Physical Properties of Rocks, v. II, edited by Carmichael, R. S., CRC Press, Boca Raton, Florida, 2, 229–287, 1982.

Davis, A., Marshak, A., Wiscombe, W., and Cahalan, R.: Multifractal characterizations of nonstationarity and intermittency in geophysical fields: Observed, retrieved or simulated, J. Geophys. Res., 99, 8055–8072, 1994.

Dolan, S., Bean, C., and Riollet, B.: The broad-band fractal nature of heterogeneity in the upper crust from petrophysical logs, Geophys. J. Int., 132, 489–507, 1998.

Dubois, J.: Non-linear Dynamics in Geophysics, John Wiley & Sons, Chichester, England, 1998.

Feder, J.: Fractals, Plenum Press, New York, 1988.

Fisher, F.: Geochemical data and sample locality maps from the Stinkingwater Mining Region, Park County, Wyoming, US Geological Survey Report USGS-GD-71-003, Tech. Rep. Rept. PB1-96987, US Dept. Commerce Natl. Tech. Inf. Service, 1971.

Fisher, F.: Tertiary mineralization and hydrothermal alteration in the Stinkingwater Mining Region, Park County, Wyoming, US Geological Survey Bulletin, 1332-C, 33, 1972.

Fisher, F.: Porphyry copper deposits associated with the Needle Creek igneous center, southern Absaroka Mountains, Wyoming, in: Symposium volume 1982, Genesis of Rocky Mountain Ore Deposits, Denver Region Exploration Geologists Society, Denver, CO, 87–93, 1983.

Fowler, A.: Mineral crystallinity in igneous rocks, in: Fractals in the Earth Sciences, edited by Barton, C. and LaPointe, P., Plenum Press, New York, 237–249, 1995.

Gettings, M.: Cantor set models of magnetic sources, Abstracts Week B, XXI General Assembly of the International Union of Geodesy and Geophysics, Boulder, Colorado, p. B193, 1995.

Gettings, M.: An Interpretation of the 1996 Aeromagnetic Data for the Santa Cruz basin, Tumacacori Mountains, Santa Rita Mountains, and Patagonia Mountains, South-Central Arizona, US Geological Survey Open-File Report 02-99, available only on http://geopubs.wr.usgs.gov/open-file/of02-99/, 2002.

Gettings, M.: A dataset of magnetic susceptibility, metalization, and alteration for samples from the Stinkingwater Mining District, Absaroka Mountains, Wyoming, US Geological Survey Open-File Report 04-1253, available only on http://pubs.usgs.gov/of/2004/1253/, 2004.

Gettings, M., Bultman, M., and Fisher, F.: Detailed profiles of southeastern Arizona obtained by a truck-mounted magnetometer – a step toward better utilization of the information content of geophysical data, US Geological Survey Circular 1062, 31–32, 1991.

Gregotski, M., Jensen, O., and Arkani-Hamed, J.: Fractal stochastic models of aeromagnetic data, Geophysics, 56, 1706–1715, 1991.

Jeffreys, H.: Theory of probability, Oxford University Press, Oxford, UK, 3 edn., 1961.

Lovejoy, S., Pecknold, S., and Schertzer, D.: Stratified multifractal magnetization and surface geomagnetic fields-I. Spectral analysis and modelling, Geophys. J. Int., 145, 112–126, 2001.

Lowell, J. and Guilbert, J.: Lateral and vertical alteration-mineralization zoning in porphyry copper deposits, Econ. Geol., 65, 363–408, 1970.

Mandelbrot, B.: Fractals: Form, Chance, and Dimension, W. H. Freeman, San Francisco, 1977.

Mandelbrot, B.: The Fractal Geometry of Nature, W. H. Freeman, San Francisco, 1982.

Mandelbrot, B.: Multifractals and $1/f$ noise, Springer Verlag, New York, 1999.

Maus, S.: Variogram analysis of magnetic and gravity data, Geophysics, 64, 776–784, 1999.

Maus, S. and Dimri, V.: Scaling properties of potential fields due to scaling sources, Geophys. Res. Lett., 21, 891–894, 1994.

Maus, S. and Dimri, V.: Potential field power spectrum inversion for scaling geology, J. Geophys. Res., 100, 12 605–12 616, 1995.

Maus, S. and Dimri, V.: Depth estimation from the scaling power spectrum of potential fields?, Geophys. J. Int., 124, 113–120, 1996.

Maus, S., Gordon, D., and Fairhead, D.: Curie-temperature depth estimation using a self-similar magnetization model, Geophys. J. Int., 129, 163–168, 1997.

Monin, A. and Yaglom, A.: Statistical Fluid Mechanics: Mechanics of Turbulence, vol. 2, MIT Press, Cambridge, Mass., 1975.

Ouillon, G., Castaing, C., and Sornette, D.: Heirarchical geometrry of faulting, J. Geophys. Res., 101, 5477–5487, 1996.

Pecknold, S., Lovejoy, S., and Schertzer, D.: Stratified multifractal magnetization and surface geomagnetic fields-II, Multifractal analysis and simulations, Geophys. J. Int., 145, 127–144, 2001.

Phelps-Dodge Corporation: Alteration maps, Needle Creek property, 1968.

Pilkington, M. and Todoeschuck, J.: Fractal magnetization of continental crust, Geophys. Res. Lett., 20, 639–641, 1993.

Pilkington, M. and Todoeschuck, J.: Scaling nature of crustal susceptibilities, Geophys. Res. Lett., 22, 779–782, 1995.

Pilkington, M., Gregotski, M., and Todoeschuck, J.: Using fractal crustal magnetization models in magnetic interpretation, Geophys. Prosp., 42, 677–692, 1994.

Quarta, T., Fedi, M., and DeSantis, A.: Source ambiguity from estimation of the scaling exponent of potenntial field power spectra, Geophys. J. Int., 140, 311–323, 2000.

Schertzer, D. and Lovejoy, S.: Physical modeling and analysis of rain and clouds by anisotropic scaling of multiplicative cascades, J. Geophys. Res., 92, 9693–9714, 1987.

Schertzer, D. and Lovejoy, S.: Nonlinear geodynamical variability: multiple singularities, universality and observables, in: Non-Linear Variability in Geophysics: Scaling and Fractals, edited by: Schertzer, D. and Lovejoy, S., Kluwer Academic, Norwell, Mass., 41–82, 1991.

Schertzer, D. and Lovejoy, S.: Universal multifractals do exist!: comments on "A statistical study of mesoscale rainfall as a random cascade", J. Appl. Meteorl., 36, 1296–1303, 1997.

Schmitt, F., Lovejoy, S., and Schertzer, D.: Multifractal analysis of the Greenland Ice-core project climate data, Geophys. Res. Lett., 22, 1689–1692, 1995.

Sornette, A., Davy, P., and Sornette, D.: Fault growth in brittle-ductile experiments and the mechanics of continental collisions, J. Gephys. Res., 98, 12 111–12 139, 1993.

Tessier, Y., Lovejoy, S., Hubert, P., Schertzer, D., and Pecknold, S.: Multifractal analysis and modeling of rainfall and river flows and scaling, causal transfer functions, J. Geophys. Res., 101, 26 427–26 440, 1996.

Tricot, C.: Curves and Fractal Dimension, Springer Verlag, New York, 1995.

Turcotte, D.: Fractals and Chaos in Geology and Geophysics, Cambridge University Press, Cambridge, UK, 2 edn., 1997.

Turcotte, D. and Huang, J.: Fractal distributions in geology, scale invariance, and deterministic chaos, in: Fractals in the Earth Sciences, edited by: Barton, C. and LaPointe, P., Plenum Press, New York, 1–38, 1995.

Zhou, S. and Thybo, H.: Power spectra analysis of geomagnetic data and KTB susceptibility logs and their implications for fractal behaviour of crustal magnetization, Pageoph., 151, 147–159, 1998.